A Differential Series-fed Dipole Array for D-band Sensing in Wafer Level Package Technology

Martijn de Kok[1], Paola A. Escobari Vargas[1], Elmine Meyer[1], Friedrich Müller[2], Tanja Braun[2], Ad C. F. Reniers[1], and Ulf Johannsen[1]
[1]Electromagnetics Group, Eindhoven University of Technology (TU/e), Eindhoven, The Netherlands
[2]Department of System Integration & Interconnection Technologies, Fraunhofer IZM, Berlin, Germany
m.d.kok@tue.nl

***Abstract*—This paper presents the design and characterization of a series-fed differential Antenna-in-Package (AiP) design, demonstrated as a four- and a six-element reflector-backed linear dipole array, that has been realized in a resin-based fan-out wafer level package technology. The four- and six-element designs achieve −10 dB input reflection bandwidths of 5.5 and 5.9 percent, realized gains of 14 and 15.4 dBi, and side-lobe levels of −10.7 and −12.1 dB, respectively. The realized samples were characterized through probed measurements in a state-of-the-art millimeter-wave anechoic chamber. After taking the RF-probe influence on the antenna performance into consideration, the measurements corroborated the simulated results.**

***Index Terms*—Antenna-in-package, Differential antenna, Reflector-backed dipole, Fan-out wafer level package, D-band**

I. INTRODUCTION

The D-band (110-170 GHz) has been the subject of increased research and interest in recent years. Sensors beyond 100 GHz, most notably short-range radars operating in the 122 GHz ISM-band, can already be found in literature [1], [2]. Moreover, academia and industry are already looking towards D-band radars, with sufficient available bandwidth for cm-level range resolutions, as a successor to the 77 GHz devices that are now solidly established in the automotive sector [3], [4].

In [5], an overview is presented of reported gain-to-area performances of D-band antennas integrated on printed circuit board (PCB), in-package, and on-chip. Antenna-in-Packages (AiPs) based on integrated substrates, low-temperature co-fired ceramics (LTCC), and organic redistribution layer (RDL) technologies were concluded to outperform PCB-based and on-chip antennas in efficiency and scalability.

In this work a fan-out wafer level package (FOWLP) technology from Fraunhofer IZM is demonstrated, which achieves better tolerances than the LTCC-based antennas listed in [5] whilst enabling multi-layer designs as opposed to other RDL-technologies, as illustrated in Fig. 1. This technology has already enabled (beyond-)5G antennas at mm-wave [6], [7].

This paper presents two 110 GHz differential reflector-backed dipole arrays, that were designed and characterized for the next generation of automotive radars operating beyond 100 GHz [4]. The differential circuits under development at Eindhoven University of Technology (TU/e) feature several valuable advantages over single-ended designs, including simplified layout design thanks to the virtual ground, lower signal distortion, suppression of common-mode noise, and better power efficiency due to the doubled maximum voltage swing [8]. Differential AiPs complement this by enabling close integration without the area and power loss of a balun. The presented designs represent a beyond-state-of-the-art contribution in gain-to-area ratio to the currently limited number of high-gain differential AiPs at D-band found in literature.

II. FAN-OUT WAFER LEVEL PACKAGE TECHNOLOGY

FOWLP integrates multiple ICs by wafer level encapsulation, forming a reconfigured wafer. A redistribution layer is then used to connect the ICs. The active area of the package is extended beyond the dies, facilitating an increased number of interconnects and embedded passive components [9].

Fraunhofer IZM has developed a technique to stack multiple metallized mold layers, to realize advanced RDLs, electromagnetic shielding, and multi-layer antennas that are located directly above the RF IC and the encapsulant to reduce the module surface area, as illustrated in Fig. 1. The sputter-coated and electroplated metallization layers are connected with laser-drilled through-mold vias, as described in [6]. The resin, which was characterized at TU/e, has a dielectric constant of 3.6 and a loss tangent of 0.0055 with a measurement accuracy of 3% [10]. An overview of the typical manufacturing parameters for direct metallization on the encapsulant is provided in Table I.

In this work, only a single mold layer with bottom- and top-side metallization is used to realize a passive demonstrator without an active chip. In Fig. 1, this is indicated as ‘Mold 2’. The vertical interconnect to feed the antenna is not considered to facilitate probe measurements. The antenna samples were manufactured alongside a variety of other structures, which predetermined the outer dimensions of 25×25 mm^2 and substrate thickness of 250 µm.

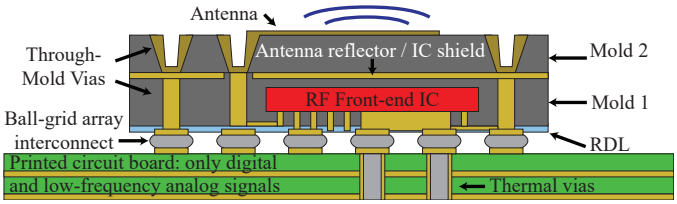

Fig. 1. Concept illustration of a FOWLP-based AiP integrated with an RF IC as a single module, based on [6].

978-88-31299-10-7/25/$31.00 ©2025 IEEE

TABLE I
TYPICAL MANUFACTURING PARAMETERS AND TOLERANCES WITHOUT OPTIMIZATION FOR DIRECT METALLIZATION ON ENCAPSULANTS

Dimension	Value [µm]	Tolerance [±µm]
Substrate thickness	250	10
Copper thickness	10	2
Via placement	–	25
Etching accuracy: traces	≥ 25	10
Etching accuracy: gaps	≥ 50	10

TABLE II
ANTENNA REQUIREMENTS WITH LINKS TO RADAR PERFORMANCE

Specification	Requirement	Radar performance
Element x-dimension	$\leq \frac{1}{2}\lambda_0$	Prevent grating lobes
Embedded element gain	≥ 15 dBi	Operating range
E-plane HPBW	$\geq 70°$	Scan range
H-plane HPBW	$\leq 12°$	Angular resolution
Bandwidth	$\geq 5\%$	Range resolution

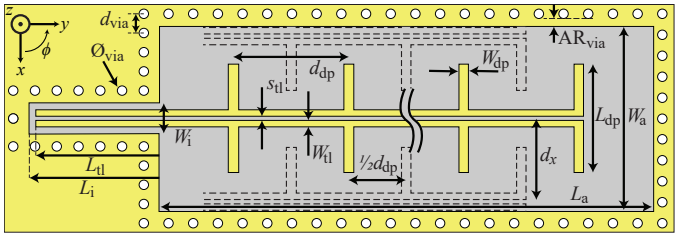

Fig. 2. Illustration of the AiP simulation model, with the indicated dimensions listed in Table III. The antennas are centered on a 250 μm thick substrate which extends to 25×25 mm in all designs and models. A reflecting metal plane covers the bottom side of the substrate. Dashed lines show adjacent element locations in an E-plane scanning array, and W_a is scaled accordingly.

III. DESIGN AND REALIZATION

A. Requirements

In this work, a high-gain fan-shaped element pattern and relative bandwidth of 5% were taken as principal design requirements as listed in Table II. Series-fed antenna structures are typically able to fulfill both requirements, making them a popular choice in contemporary automotive radar systems and also interesting options for D-band applications [3], [7]. Although a 145 GHz design would have been preferred to align with the allocated radar band, the choice of 110 GHz as center frequency was based on available lab equipment.

The antenna was specified to interface with mm-wave radar circuits under development at TU/e with a standard differential impedance of 100 Ω, eliminating the need for a lossy impedance transformer and balun between AiP and IC.

B. Design

The starting point of the proposed AiP was a scaled version of the dipole antenna presented in [11], where the bottom metalization acts as a reflector instead of a ground plane. The resulting design is presented in Fig. 2. A total of six reflector-backed dipole elements are placed in series, with the length and width of the elements tuned in CST to achieve a 100 Ω match at the center frequency of 110 GHz. The dipoles are approximately one guided wavelength long, exceeding the $0.5\lambda_0$ element size requirement specified in Table II. However, this can be remedied through a staggered array grid. The element spacing d_{dp} at approximately one guided wavelength ensures all elements radiate in-phase at the center frequency.

TABLE III
ANTENNA DIMENSIONS CORRESPONDING TO FIG. 2

Dimension	Symbol	Value [µm]
Dipole length (x-dimension)	L_{dp}	1765
Dipole width (y-dimension)	W_{dp}	150
Dipole element spacing	d_{dp}	1865
Transmission line length	L_{tl}	2000
Transmission line conductor width	W_{tl}	100
Transmission line conductor gap	s_{tl}	70
Input aperture length	L_i	2100
Input aperture width	W_i	500
Aperture width	W_a	3000
Aperture length (4 elements)	L_{a4}	8000
Aperture length (6 elements)	L_{a6}	12000
Fence via spacing	d_{via}	310 – 400
Fence via diameter	$ø_{via}$	150
Fence via annular ring	AR_{via}	125

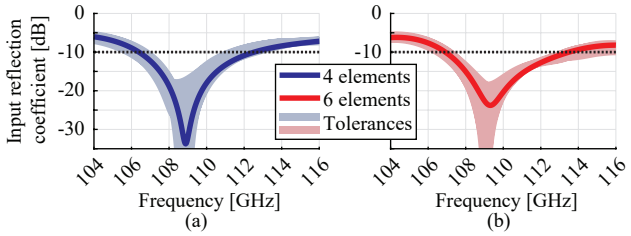

Fig. 3. Simulated input reflection coefficients of the four-element (a) and six-element (b) designs, with the ranges indicating maximum variations due to manufacturing tolerances. Reference impedance: 100 Ω.

The antenna array is enclosed by a fence of through-mold vias to prevent the leaky wave contribution in the resin substrate from reaching the edge of the sample and causing spurious edge radiation. This fence was placed sufficiently far from the dipoles for the drilling tolerances to be negligible on the performance, which was verified using CST.

C. Simulated performance

The simulated input reflection coefficients of the four- and six-element antennas are depicted in Fig. 3. The robustness of the design against all combinations of extreme tolerance values listed in Table I was assessed through a parameter sweep. Based on the nominal performance, the four- and six-element designs are expected to achieve −10 dB input reflection bandwidths of 6 and 6.5 GHz or 5.5% and 5.9%, respectively, achieving the 5% requirement with margin. The variations due to tolerances indicate a possible shift in operating frequency limited to around ±0.5 GHz, or ±0.5%.

The simulated farfield patterns are depicted in Fig. 4. The nominal designs are expected to reach realized gain levels of 14 and 15.4 dBi at the center frequency, with indicated radiation efficiencies of 79% and 77%, respectively. This matches the expected gain difference of 1.4 dB based on the antenna dimensions, which indicates the antenna scales efficiently. The four-element AiP achieves a peak side lobe level (SLL) of −10.7 dB, and the six-element design −12.1 dB.

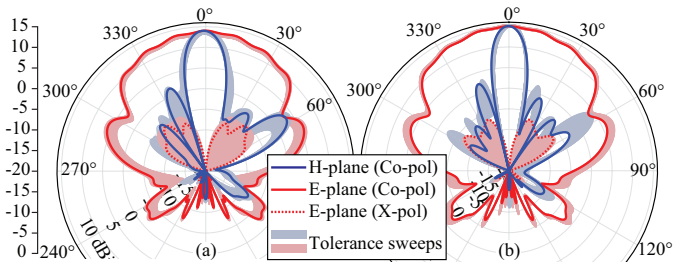

Fig. 4. Simulated realized-gain farfield patterns of the four-element (a) and six-element (b) designs at 110 GHz, with the ranges indicating maximum variations due to manufacturing tolerances. The cross- polarized (X-pol) component in the H-plane does not exceed −35 dBi.

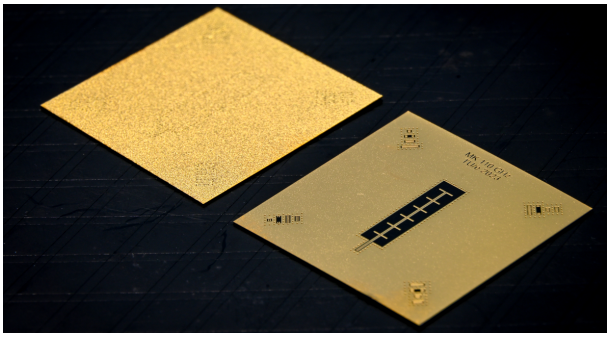

Fig. 5. Realized six-element samples. Sample size is 25×25 mm^2.

D. Realization

Fig. 5 shows a realized six-element sample. After manufacturing, the etching tolerances were observed to be slightly higher than expected at a maximum variation of ±20 µm. The realized average copper layer thickness before the surface finish is 12.4 µm with a peak standard deviation of 0.82 µm. The realized resin substrate thickness was measured to be within a 225 to 250 µm range. These values are slightly outside of the ranges considered in the design process but will be taken into account in the discussion of measurement results. It should be noted that manufacturing was done on a multi-project wafer without optimization to specific designs, which could be improved to achieve better tolerances and yield.

IV. MEASUREMENTS

A. Farfields: mm-Wave anechoic chamber

Key to the measurement campaign of the presented D-band antenna samples is the novel mm-wave anechoic chamber that was developed in-house at TU/e [12]. As shown in Fig. 6, the antenna under test (AUT) is placed on a pedestal at the center of the compact spherical chamber, which is equipped with a probe station. A rail-based reference antenna can scan around the AUT to create a farfield pattern cut along the θ-axis between ±125° [13]. Moreover, the entire spherical chamber can rotate 180° along the ϕ-axis to characterize a 3D-pattern.

RF-probes can have a significant impact on the radiating performance of an antenna, especially at mm-wave frequencies. This is due to parasitic radiation at the probe tips and reflections by the nearby bulky probe-body. To minimize

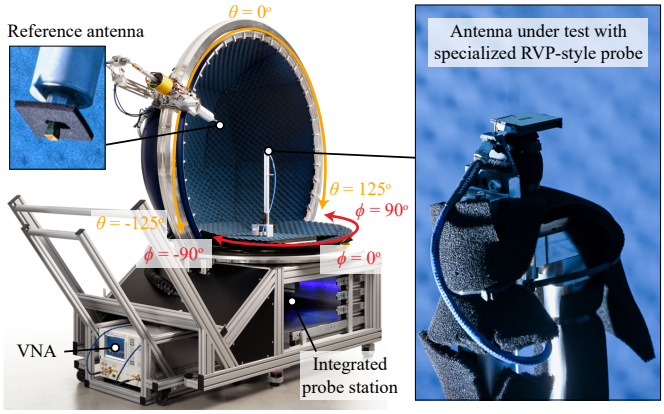

Fig. 6. The mm-wave anechoic chamber, half-open for illustration purposes.

the disturbance caused by the body, a custom variation of Picoprobe's RVP-style probe introduced in [14] is used that positions the probe body below the antenna as shown in Fig. 6. The available probe has 100 µm-pitch ground-signal (GS) tips, and a 1.0 mm RF-connector that is rated for mode-free operation up to 110 GHz. As the chamber only supports single probes at the time of writing, a Short-Open-Load (SOL)-calibration was performed at the probe tips.

B. Realized gain

A reference horn antenna with known realized gain is placed in the AUT position. After taking a series of transmission measurements whilst varying the radial distance between the two antennas from 130 to 190 mm, the distance between the antenna amplitude centers is determined by fitting the Friis equation. With all other variables known, the total power loss in waveguides, cables, and transitions was determined. After characterizing the setup losses, the process was repeated with the AUTs to determine their realized gain relative to the reference horn antenna.

C. Modeling of probe influence

Despite the bulk of its body being outside the field of view of the AiP, the housing of the GS RF-probe used in the mm-wave anechoic chamber was expected to have a considerable influence on the radiated measurement results.

The parasitic radiation of the probe was characterized by landing on the 50 Ω load calibration standard and measuring the farfield pattern and realized gain using the methods described in this section. Based on the measurements, this parasitic radiation is expected to limit the reliably measurable realized AUT gain, or null depth, to ≥ -15 dBi. This was considered to be sufficiently low to reliably measure the main beam and primary side lobes, but the interfering radiation causes ripples in the lower side lobes and X-pol patterns. The GS configuration is expected to cause an asymmetry in the antenna excitation. A model of the probe was co-simulated in CST to characterize its influence on the measurement results.

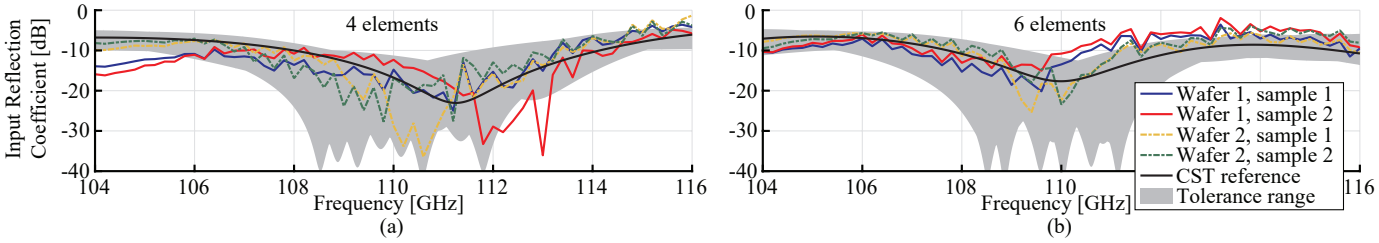

Fig. 7. Measured input reflection magnitude for a 100 Ω reference impedance four-element (a) and six-element (b) antennas. A range of simulation results based on manufacturing and measurement tolerances is shaded grey. The CST reference includes the feed point offset, the measured decreased substrate thickness, and the increased copper thickness. The probe was not co-simulated in this case.

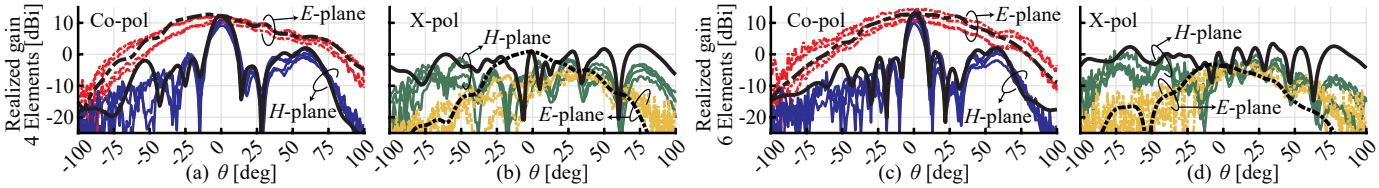

Fig. 8. Measured co- (Co-pol) and cross-polarized (X-pol) realized-gain patterns at 110 GHz of four-element (a-b) and six-element (c-d) samples, two samples per wafer for both designs. The CST reference simulations (in black) include the GS-probe. Results at 107.5 and 112.5 GHz were omitted for brevity.

V. RESULTS

A. Input reflection and impedance

The measured input reflection parameters and impedances of the four- and six-element AiPs are shown in Fig. 7. The measurements indicated a significant sensitivity to the exact placement of the probe. Whilst the original model in CST was based on a discrete port at the tips of the input transmission line, the probe position can be up to approximately 100 µm away from the edge. This forms a capacitive stub that de-tunes the antenna and shifts the resonance frequency.

Moreover, the permittivity characterization was performed with an accuracy of up to ±3%, which could account for a shift in resonance frequency of up to 1 GHz or around 1% of the designed frequency. From the results in Fig. 7, a variation can be discerned between the samples in wafers 1 and 2, whilst the sample pairs within each wafer are more consistent. Ongoing research on the characterization of the FOWLP technology is expected to reduce manufacturing variations in the future. The measured variations in probe position, dielectric constant, etching, and substrate thickness were considered to simulate the ranges that are depicted in grey in Fig. 7.

B. Farfield radiation patterns

The measured radiation pattern cuts in the E- ($\phi = 0°$) and H-planes ($\phi = 90°$) are shown in Fig. 8 for 110 GHz. The realized gain measurements at broadside were used to re-normalize the farfield measurements. The patterns show excellent agreement with simulations, with better null and main beam alignment than examples from other works such as [2], [7]. The CST reference is based on the nominal design parameters, with the GS probe tips located at 75 µm from the start of the transmission line. Particularly the measured asymmetries in the co-polarized E-plane ripple and the cross-polarized H-plane pattern, both absent from the nominal simulation without RF-probe, match the simulations well.

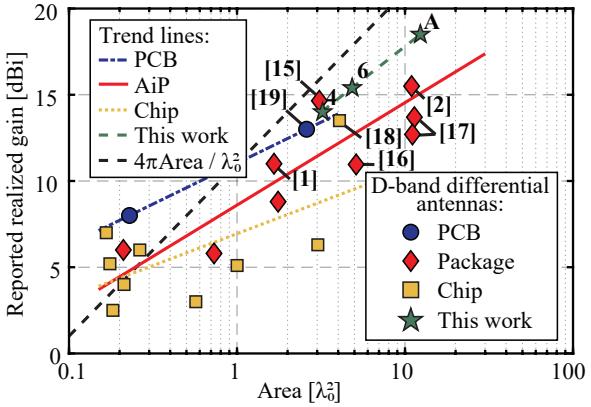

Fig. 9. Overview of reported realized gain performances of differential D-band antennas from literature, adapted from [5]. The antennas presented in this work are labeled as '4,' '6' (denoting elements) and 'A' (4×6 array).

C. State-of-the-art comparison and outlook

The overview from [5] was re-made to focus on differential designs in Fig. 9. The performances presented in this work are included in the graph as well. They are marked with '4' and '6' in Fig. 9 to denote their element counts. Note that [15] and [16], [17] are differential radiators, but have waveguide-based and single-ended interfaces, respectively.

Although the effective aperture of small antennas can exceed their physical size, for higher-gain designs a trend close to the ideal $4\pi\text{Area}/\lambda_0$-line indicates efficient scalability of the design and technology with limited decrease in radiation efficiency. With $L_a \times W_a$ taken as areas, the designs presented in this work outperform the area-gain trends of other differential PCB-, chip- and package-based antennas at D-band. The only high-gain design exceeding the trend is [15], which is a corporate-fed end-fire dipole array in a metal fixture. This is a promising concept with expandability to 2D scanning, but

TABLE IV
COMPARISON OF DIFFERENTIAL D-BAND ANTENNAS FROM LITERATURE.

Design		f_c [GHz]	Size $[\lambda_0 \times \lambda_0]$	Gain [dBi]	η_{ant} [%]	BW [%]	Source
4×4 on-chip dipoles		110	2.0×2.0	13.5	45	7.3	[18]
8-element rhombic AiP		120	1.5×1.1	11	-	5	[1]
43-element rhombic AiP		120	5.5×2.0	15.5	75	4.9	[2]
1×8 series-fed patch		123.5	5.7×0.5	13	90	5.7	[19]
1×8 end-fire dipole array in metal fixture		145	3.9×0.8	14.7	70	41.4	[15]
AiP patch arrays	2×2	139.5	2.26×2.26	11	65	22.2	[16]
with balun:	2×4	137.7	4.1×2.8	13.7	45.2	32.7	[17]
Series-fed	1×4	110	1.1×2.9	14	79	5.5	**This**
dipole array	1×6	110	1.1×4.4	15.4	77	5.9	**work**
designs:	4×6	110	2.6×4.7	18.5	74	4.5	

not directly implementable as a low-profile package on PCB.

The limited subset of integrated antennas with over 10 dBi of reported realized gain is listed in more detail in Table IV. Notable among the differential AiPs are the 120 GHz 8-element and 43-element rhombic arrays from [1] and [2], respectively. These designs are implemented in a wafer-level ball grid array technology, and report 11 and 15.5 dBi of realized gain respectively. Compared to these designs, the multi-layer capability of the FOWLP technology used in this work enables a larger degree of design freedom and area savings. Moreover, unlike the fixed-gain rhombic arrays, the series-fed dipoles can be configured in a linear array to further increase gain, improve angular resolution, and enable E-plane beam-steering. The simulated broadside performance of a four-by-six array was included in Table IV and Fig. 9. Without any adjustments to the element design, a simulated scan loss of less than 1 dB was achieved within a scan range of $\pm 40°$, although these results had to be omitted for the sake of brevity. Note that the array aperture, and therefore its gain, is not four times larger than the 6-element design due to the staggered grid.

VI. CONCLUSION

The design of a D-band differential reflector-backed dipole array antenna in a FOWLP technology has been presented. The four- and six-element series-fed designs operate with a 6% bandwidth around 110 GHz and serve as proofs of concept of highly integrated radar components beyond 100 GHz.

The antennas were characterized through probe-based measurements in a state-of-the-art anechoic measurement chamber. The presented antenna performance represent an advancement over the limited number of previously published package-based differential antennas operating at D-band, demonstrating excellent gain-over-area performance beyond the state-of-the-art. The broadside radiation perpendicular to the PCB plane, combined with the manufacturing precision and efficient scalability offered by the technology and the potential to expand towards a scanning array sets the design apart from other previously published works in this frequency range.

Based on the efficient scalability and the achievable manufacturing tolerances, the FOWLP technology is considered a promising candidate to realize highly integrated front-end modules for the beyond-100 GHz era of automotive radars.

ACKNOWLEDGMENT

This document is a result of the NEXTPERCEPTION project, which is jointly funded by the European Commission and national funding agencies under the ECSEL joint undertaking. Part of the work is co-funded by the PENTA-EURIPIDES 2021 project InnoStar. The authors would like to thank Noah Reniers for his help with the measurements.

REFERENCES

[1] M. Furqan, F. Ahmed, R. Feger, K. Aufinger, W. Hartner, and A. Stelzer, "A SiGe-based fully-integrated 122-GHz FMCW radar sensor in an eWLB package," *International Journal on Microwave and Wireless Technologies*, vol. 9, no. 6, p. 1219–1230, 2017.

[2] M. Furqan, F. Ahmed, and A. Stelzer, "A SiGe 122-GHz FMCW radar sensor with 21.5 dBm EIRP based on a 43-element antenna array in an eWLB package," in *IEEE MTT-S International Conference on Microwaves for Intelligent Mobility*, 2018, pp. 1–4.

[3] M. Köhler, J. Hasch, H. Bloecher, and L.-P. Schmidt, "Feasibility of automotive radar at frequencies beyond 100 GHz," *International Journal on Microwave and Wireless Technologies*, vol. 5, Feb 2013.

[4] V. Vidojkovic *et al.*, "RF and mm-wave systems and circuits for communications and sensing," in *2023 58th International Scientific Conference on Information, Communication and Energy Systems and Technologies (ICEST)*, 2023, pp. 83–92.

[5] M. de Kok, A. B. Smolders, and U. Johannsen, "A review of design and integration technologies for D-band antennas," *IEEE Open Journal on Antennas and Propagation*, vol. 2, pp. 746–758, 2021.

[6] T. Braun *et al.*, "Development of a scalable AiP module for mmWave 5G MIMO applications based on a double molded FOWLP approach," in *IEEE Electronic Components and Technology Conf*, 2021, pp. 1–7.

[7] T. H. Le *et al.*, "Design, fabrication and measurement of FOWLP-based series-fed antennas for 6G D-band MIMO applications," in *IEEE 9th Electronics System-Integration Technology Conference*, 2022, pp. 1–4.

[8] M. Zhao, "Differential interfaces improve performance in RF transceiver designs," *Analog Dialogue*, vol. 45, no. 7, Jul 2011.

[9] T. Braun *et al.*, "Fan-out wafer level packaging for 5G and mm-Wave applications," in *International Conference on Electronics Packaging and iMAPS All Asia Conference (ICEP-IAAC)*, 2018, pp. 247–251.

[10] P. A. Escobari Vargas, "Packaging technology characterization for 5G antenna-in-package and filter-in-package application," EngD Thesis, Eindhoven University of Technology, Feb. 2024.

[11] U. Johannsen *et al.*, "Integrated antenna concept for millimeter-wave front-end modules in proven technologies," in *6th European Conference on Antennas and Propagation (EuCAP)*, 2012, pp. 2560–2563.

[12] A. C. F. Reniers *et al.*, "Spherical mm-wave anechoic chamber for accurate far-field radiation pattern measurements," in *2022 52nd European Microwave Conference (EuMC)*, 2022, pp. 318–321.

[13] P. Yadav, L. A. Bronckers, A. B. Smolders, and A. C. Reniers, "Uncertainties in the estimation of the gain of a standard gain horn in the frequency range of 90 GHz to 140 GHz," in *18th European Conference on Antennas and Propagation*, 2024, pp. 1–5.

[14] A. C. F. Reniers *et al.*, "The influence of the probe connection on mm-wave antenna measurements," *IEEE Transactions on Antennas and Propagation*, vol. 63, no. 9, pp. 3819–3825, 2015.

[15] Y. W. Kim, Y. K. Koh, and M. Kim, "Microstrip array antennas packaged in metal fixture for 150 GHz beamforming applications," *IEEE Antennas and Wireless Propagation Letters*, vol. 23, no. 3, pp. 1055–1059, 2024.

[16] X. Wang *et al.*, "Broadband D-band patch antenna array in wafer-level package based on BCB process," *IEEE Open Journal of Antennas and Propagation*, vol. 3, pp. 1172–1179, 2022.

[17] X. Wang, G. Xiao, B. Zhao, Y. Huang, and Q. Xu, "A broadband D-band cavity-backed coupled-feed patch antenna in wafer-level package based on heterogeneous integrations," *IEEE Transactions on Antennas and Propagation*, vol. 72, no. 8, pp. 6298–6308, 2024.

[18] W. Shin, B. Ku, O. Inac, Y. Ou, and G. M. Rebeiz, "A 108–114 GHz 4 ×4 wafer-scale phased array transmitter with high-efficiency on-chip antennas," *IEEE Journal of Solid-State Circuits*, vol. 48, no. 9, 2013.

[19] R. Hasan, W. A. Ahmed, J. Lu, H. J. Ng, and D. Kissinger, "F-Band Differential Microstrip Patch Antenna Array and Waveguide to Differential Microstrip Line Transition for FMCW Radar Sensor," *IEEE Sensors Journal*, vol. 19, no. 15, pp. 6486–6496, 2019.